

## High-resolution projections of extreme heat in New York City

L. Ortiz<sup>1,\*</sup>, J. E. González<sup>1</sup>, R. Horton<sup>2</sup>, W. Lin<sup>3</sup>, W. Wu<sup>4</sup>, P. Ramamurthy<sup>1</sup>, M. Arend<sup>1</sup>, and R. Bornstein<sup>5</sup>

1. Mechanical Engineering Department, The City College of New York, New York, NY 10031 (\*Contact: [lortiz10@citymail.cuny.edu](mailto:lortiz10@citymail.cuny.edu))
2. Lamont-Doherty Earth Observatory, Columbia University Earth Institute, New York, NY 10964
3. Environmental & Climate Sciences Department, Brookhaven National Laboratory, Upton, NY 11973
4. Coast Survey Development Laboratory, Office of Coast Survey, National Ocean Service, NOAA, Silver Spring, MD 20910
5. Meteorology Department, San Jose State University, San Jose, CA, 95192

### Abstract

Heat waves impact a wide array of human activity, including health, cooling energy demand, and infrastructure. Cities amplify many of these impacts by concentrating large populations and critical infrastructure in relatively small areas. In addition, heat waves are expected to become longer, more intense, and more frequent in North America. Here, we evaluate combined climate and urban surface impacts on localized heat wave metrics throughout the 21<sup>st</sup> century across two emissions scenarios (RCP4.5 and RCP8.5) for New York City (NYC), which houses the largest urban population in the United States. We account for local biases due to urban surfaces via bias correcting with observed records and urbanized 1 km resolution dynamical downscaling simulations across selected time periods (2045-2049 and 2095-2099). Analysis of statistically downscaled global model output shows underestimation of uncorrected summer daily maximum temperatures, leading to lower heat wave intensity and duration projections. High resolution dynamical downscaling simulations reveal strong dependency of changes in event duration and intensity on geographical location and urban density. Event intensity changes are expected to be highest closer to the coast, where afternoon sea-breezes have traditionally mitigated summer high temperatures. Meanwhile, event duration anomaly is largest over Manhattan, where the urban canopy is denser and taller.

**Keywords:** heat waves, dynamical downscaling, urban, climate impacts, climate projections

This article has been accepted for publication and undergone full peer review but has not been through the copyediting, typesetting, pagination and proofreading process, which may lead to differences between this version and the Version of Record. Please cite this article as doi: 10.1002/joc.6102

## 1. Introduction

Heat waves caused the second most weather related fatalities in the US in the last decade (National Weather Service, 2015), with 97 directly attributed deaths per year between 2008-2017 and 107 in 2017 alone. NYC is the most heavily populated city in the US, with over 8 million residents, more than double of the second highest population, Los Angeles. Studies have shown that longer, more intense heat waves in the US are associated with increases in mortality (Anderson and Bell, 2010), metrics that are projected to increase throughout the 21<sup>st</sup> century (Meehl and Tebaldi, 2004). Further, these summertime increases in heat-related mortality may not be offset by decreases in cold-weather deaths in Manhattan, New York (Li et al., 2013), the city's most densely populated borough. Warm weather also increases energy demand for air conditioning (Le Comte and Warren, 1981; Miller et al., 2008; Ortiz et al., 2018a; Santamouris et al., 2001), although decreases in winter heating may partially or completely offset the cost of increased cooling (Rosenthal et al., 1995). Infrastructure and health impacts may also occur simultaneously, as was shown for the 2003 NYC city-wide blackout, which saw a 25% increase in non-accidental deaths (Anderson and Bell, 2012). In addition, cities interact with the atmospheric boundary layer by introducing heat source and storage terms into the surface energy balance (Oke, 1988) and limiting natural cooling processes (e.g., soil moisture evaporation). These processes, in general, lead to higher temperatures in cities compared to surrounding suburban and rural areas, a phenomenon called the urban heat island (UHI). These added surface energy terms modify the atmospheric boundary layer, potentially increasing convective motions, elevating the daytime convective layer and weakening nighttime stable layers. In NYC, the complex nature of its urban landscape and its geographical location has historically led to a spatially and temporally heterogeneous UHI (Gaffin et al., 2008).

Urban surface-atmosphere feedbacks can exacerbate heat wave conditions in cities. For

example, Li and Bou-Zeid (2013) found UHI intensification in the Baltimore, Maryland, USA area, while Ramamurthy et al (2017) found the NYC UHI reached up to 10°C during the June 2016 heat wave, both attributing synergistic interactions between heat waves and urban surfaces to decreased evaporative cooling over cities. In the July 3-8, 2010 heat wave in NYC, urban contributions to afternoon near surface temperatures were 2°C larger than on preceding days (Ortiz et al., 2018b), due to a combination of decreased evaporative cooling, modified wind speeds, and increased anthropogenic heat. Li et al (2016) found enhancement of the Beijing Metropolitan Area UHI due to wind profile changes during heat waves, similar to results from Founda and Santamouris (2017), who found UHI intensification in Athens, Greece to be highly dependent on wind magnitude and direction. Others have found evidence of UHI intensification during heat waves in Madison, Wisconsin, USA (1.8°C daytime, 5.3°C nighttime) (Schatz and Kucharik, 2015). However, Scott et al. (2018) showed in a multi-city, multi-year study that in 70% of the cities analyzed, rural temperatures increased faster than urban temperatures, leading to lower UHI magnitudes during warm days. This underscores the need for studies of the underlying land surface processes that determine urban temperatures during hot days, and how they vary across different regions and urban forms. Meanwhile, study of climate impacts and development of future projections has traditionally relied on General Circulation Models (GCMs), which operate at spatial resolutions of ~100 km. While useful to evaluate global and even continental scale climate impacts, their coarse grid spacing limits their potential to represent locally significant processes due to complex orography, coastlines, and heterogeneous land cover (e.g. cities), as well as fine scale atmospheric processes (e.g. clouds, convection). Attempts to overcome these limitations often involve downscaling techniques to add information at finer scales than GCM native grids. There are two approaches to achieve this: statistical and dynamical. The former often involves using extraneous climatological records to transform coarse GCM output to more

closely match records at specific locations, often by transforming their distribution.

Dynamical downscaling uses GCM output as initial and boundary conditions to a limited area numerical weather prediction system, which then solves the systems of equations describing the behavior of the land surface and atmosphere. Here, we present projections based both on a statistically downscaled GCM ensemble as well as high resolution (1 km horizontal grid spacing) dynamical downscaling to explore temporal and geospatial variability of heat wave metrics throughout the 21<sup>st</sup> century. Our approach aims to incorporate urban surface processes that may not be adequately represented in GCMs due to limitations in model resolution and parameterizations.

## 2. Methods

### 2.1. Heat wave definitions

There is no definite definition of a heat wave, with various definitions found in the literature addressing the needs of particular communities. Smith et al. (2013) showed that in the US Northeast, heat wave days have increased across 15 definitions. Here, we define a heat wave following regional US National Weather Service in New York, which labels a heat wave as at least 3 consecutive days with temperatures of at least 90°F (32.22°C) (National Weather Service, 2018). However, minimum temperatures have been shown to Results will use two metrics to describe heat wave projections:

- **Mean heat wave intensity:** Mean daily maximum temperature (°C) of all events in a given year.
- **Mean heat wave duration:** Mean heat wave duration, in days, of all events in a given year.

### 2.2. Observations and GCM Ensemble

Observation records within New York City were taken from the Global Historical Climatological Network (GHCN)-Daily (Menne et al., 2012) weather stations, specifically at Central Park, John F. Kennedy Airport (JFK), and LaGuardia Airport (LGA). These stations were selected for having long, mostly uninterrupted measurement periods spanning multiple decades. GHCN-Daily records are quality-checked, but not homogenized. Although all three stations are located within NYC city limits, differences in their surrounding land cover characteristics and distance to the coast impact each record's temperatures. For example, Central Park station, although located within the densely packed borough of Manhattan, is surrounded by grass and trees, whereas LGA and JFK are located close to the north and south shores of Queens borough (Figure 1, insert), respectively.

Ensemble members used in the single point statistically downscaled projections belong to the Fifth Climate Model Inter-comparison Project (CMIP5) (Taylor et al., 2012) and are detailed in Table 1. For each model, we consider daily maximum temperature from the summers (June-July-August) between 2006-2100. Two scenarios are considered based on the Representative Concentration Pathways (van Vuuren et al., 2011), RCP4.5 and RCP8.5, which use a combination of policy, technology, and demographic projections to estimate global radiative forcing paths. RCP4.5 (Thomson et al., 2011) is considered a medium emissions scenario, with increasing global radiative forcing that stabilizes by 2100 at 4.5 W/m<sup>2</sup>. RCP8.5 (Riahi et al., 2011) is a high emission or “business as usual” scenario, with increasing radiative forcing reaching around 8.5 W/m<sup>2</sup> by end of century.

### [Tab. 1]

#### **2.3. Statistical bias-correction**

Mean event duration (days/event) and intensity (event maximum temperature) were computed using a composite temperature record based on the daily maximum temperature

averaged across all three urban stations. These stations were selected due to (a) their proximity to NYC, and (b) their long, consistent records. These historical records were, in turn, used to perform bias correction GCM projections following the work of Hawkins et al., 2013 and Piani et al., 2010. The bias correction technique corrects for model mean and standard deviation using a linear model:

$$T_{BC} = \bar{T}_{Obs,REF} + \frac{\sigma_{Obs,REF}}{\sigma_{GCM,REF}} (\bar{T}_{GCM,RAW}(t) - \bar{T}_{GCM,REF})$$

Here,  $T$  refers to the temperature records, and  $\sigma$  refers to its standard deviation. Subscripts  $Obs$  and  $GCM$  refer to observation and model data, respectively, while  $REF$  and  $RAW$  refer to the reference (2006-2015) and entire projection periods (2006-2099). The over bar ( $\bar{\cdot}$ ) marker denotes use of the average for the specified dataset and time period. All three stations used were missing a minimal amount of data (<2%) which were removed from the record before computing the mean and standard deviation. Uncertainties in the projections were quantified by use of a 26-model ensemble. GCM horizontal resolution is often >100 km, so in many cases there was no grid point that coincides with NYC city limits. For all models, the geographically closest land grid point to NYC was used to develop all projections. A single point is used due to GCMs' generally coarse resolution, meaning that other grid points might be too distant to NYC to provide relevant information.

#### 2.4. Urbanized dynamical downscaling

This work uses the WRF model (Skamarock et al., 2008) to study interactions between cities and the atmosphere during extreme heat events. Model initial and boundary conditions are derived from the National Center for Atmospheric Research (NCAR) bias-corrected Community Earth System Model (CESM) dataset (Monaghan et al., 2014). This data has been bias-corrected using Era-Interim reanalysis across all vertical levels (Bruyère et al., 2014). This bias-correction method decomposes all GCM variables into a seasonal and trend

component, and then substitutes the seasonal component of the GCM with that of the reanalysis. This approach was found to improve representation of precipitation, as well as correcting cooler 2 m temperature biases by 2-3°C.

Simulations use one parent domain at 9 km grid spacing with two subsequent nested domains, each reducing grid spacing by a factor of three, reaching 1 km resolution (Figure 1). In order to account for processes critical to urban climate, an urban parameterization is required. In particular, we use the Building Effect Parameterization (BEP) developed by Martilli et al. (2002). BEP is a multi-layer urban canopy parameterization, possessing an internal coordinate system that resolves dynamical and energy fluxes between the urban canopy and the atmosphere. Urban momentum and energy fluxes are then added to adjacent WRF grid points, modifying thermodynamic and dynamical characteristics of the atmosphere. BEP represents mechanical impacts of the urban canopy as sinks in the momentum equation, as well as radiation blocking and reflection between walls and roofs. In addition to these building surface effects, we include the Building Energy Model (BEM) from Salamanca et al. (2010). This parameterization adds building envelope anthropogenic heat fluxes to BEP by modeling air conditioning demand. Air conditioning target temperature was set to 24.85°C, with a target specific humidity of 0.1 g<sub>vapor</sub>/kg<sub>air</sub>.

### [Fig. 1]

BEP and BEM have also been modified to account for latent heat fluxes from air conditioning, based on the work of Gutierrez et al. (2016) as well as effects of varying building packing density on drag coefficient (Gutiérrez et al., 2015b). Cooling towers use evaporative cooling processes to remove heat from water used in air conditioning systems. This evaporative cooling effectively partitions urban heat fluxes into sensible and latent, adding a hydrological component to BEM. Gutierrez et al, 2015b implemented impacts of building packing density into the BEP code following results from Reynolds averaged

numerical simulations (RANS) of Santiago et al. (2008), who related buildings' drag coefficient to their packing density through a series of experiments, as follows:

$$C_{eq}(\lambda_p) = \begin{cases} 3.32\lambda_p^{0.47} \text{ for } \lambda_p \leq 0.29 \\ 1.85 \text{ for } \lambda_p > 0.29 \end{cases}$$

Here,  $C_{eq}$  is the urban canopy sectional drag coefficient as a function of  $\lambda_p$ , the building area fraction. This equation was fitted from the RANS results as a compromise between accuracy and simplicity; the choice of an empirical equation cannot be physically interpreted. In order to maximize the utility of the variable drag formulation, urban canopy parameters, including building area fraction and building height were ingested into all simulation runs based on the Property Land-Use Tax-lot Output (PLUTO, Figure 2). PLUTO is a public dataset that includes building physical trait data including footprint area, number of floors, and use type. Building heights were computed by assuming a floor height of 5 m, while building area was approximated by subtracting non-floor area (e.g., parking) from lot total area. Urban canopy parameters were interpolated into the model high resolution domain with a horizontal grid spacing of 1 km. Gutierrez et al (Gutiérrez et al., 2015b) showed that these modifications and inclusion of high-resolution urban canopy parameters improved model winds and temperature vertical profiles when tested over an NYC domain. Tables 2 and 3 summarizes the physics parameterizations used in all simulations.

[**Tabs. 2-3; Fig. 2**]

### 3. Results

#### 3.1. Observed changes

As detailed in the Methods section, New York City houses three weather stations with at least 50 years of operation. The Central Park weather station has been in operation since 1869, while the LaGuardia (LGA) and John F. Kennedy (JFK) airports' records go back as far as 1939 and 1959, respectively. Summer annual mean daily maximum temperatures,

summarized in Figure 3, show increasing linear trends at a rate of 0.11°C per decade for Central Park and 0.13°C per decade for LGA, significant at  $p < 0.01$ , while JFK increases at 0.13°C per decade (not significant at  $p < 0.01$ ). JFK median temperatures are cooler than Central Park and LGA by ~1°C due to south/south-westerly sea-breeze typical to the area (Gedzelman et al., 2003). Sea-breeze patterns have been shown to be an important factor in the formation and daily cycle of the NYC UHI. Studies have found that on days when a sea-breeze develops, UHI formation is delayed, with its center pushed towards the northwest of the city and neighboring New Jersey. At night, a land breeze forms, moving the UHI center closer to the southeast coastline.

Heat waves in NYC are defined as at least three days with temperatures reaching at least 90°F (32.22°C). Station records show that the likelihood of temperatures exceeding the heat wave threshold are somewhat low, leading to non-significant trends in heat wave frequency, duration, and intensity Table 4.

[Fig. 3; Tab. 4]

### 3.2. Global model ensemble projections

Applying the bias correction technique outlined in the Methods section (Hawkins et al., 2013) to downscale each model in a 26-member ensemble reveals large cool biases in raw GCM output for NYC daily maximum records. We use kernel density estimates of daily maximum temperature for each ensemble member to quantify the impact of the statistical downscaling technique on mean and standard deviation statistics. As shown in Figure 4, models without bias-correction, in general, underestimate observations on average by 2.7°C. This may be in part due to NYC's close proximity to the ocean, which may be included in some of the GCM's grid cell area. The statistical downscaling technique modifies the distribution of each ensemble member to more closely match that of the station observations. In addition, inter-

model spread in mean and standard deviation is reduced during the reference period. Bias corrected mean daily maximum temperature (Figure 5a) shows a nearly linear trend in the high emissions scenario (RCP8.5), whereas rate of change in the stabilization scenario (RCP4.5) slows after 2040. RCP4.5 shows a linear trend of 0.3°C per decade, while RCP8.5 grows at a rate about three times faster, 0.69°C per decade. Model spread, quantified as 95% confidence intervals become slightly wider towards the latter half of the century, covering a range of <1°C, while the band is closer to 0.5°C in the first half. At least a fraction of these observed long-term increases may be due upstream urbanization in New Jersey throughout the 20<sup>th</sup> century, as transitioned from agrarian landuse to urban and suburban (Wichansky et al., 2008). Zhang et al. (2009) showed that upstream urbanization may intensify UHI magnitude. He showed that for the city of Baltimore, Maryland, USA, upstream urbanization accounted for up to 25% of the UHI magnitude. Meanwhile, uncorrected projections (Figure 5d) indicate similar increases in rate, albeit with a cooler ensemble mean. Differences between the two are larger in RCP8.5, where they grow from close to 3.25 to nearly 4.5°C by end of century, whereas in RCP4.5, their difference only changes by less than 0.5°C (Figure 5g).

#### [Figs. 4-5]

Bias corrected mean intensity, defined as the mean of event maximum temperatures in a given year (Figure 5b), grows at a rate nearly 0.3°C (RCP8.5) per decade, while the uncorrected record (Figure 5e) grows at 0.1°C per decade, nearly three times slower. RCP4.5 projections show a similar relationship between corrected and uncorrected records, although in general smaller, with 0.9 (corrected) to 0.3°C (uncorrected) per decade. Differences in ensemble mean (Figure 5h), however, grow larger over time between the two scenarios, with RCP8.5 and RCP4.5 being up to 2.5 and 1°C, respectively, over their uncorrected counterparts. Mean event duration projections (Figure 5c) are similar across RCP4.5 and

RCP8.5 up to the 2040s decade, similar to event intensity projections. Accelerating growth in projections of the latter half of the century are coupled with considerable increases in inter-model spread, with a 90% confidence band spanning ~10 days, compared to about 2 days in the first half. Average event duration in RCP8.5 grows from 5 days to over 25 days by end of century, with RCP4.5 growing from 5 to 7 days per event. This is due to both usage of a limited window for events to happen (i.e., June-July-August) as well as a constant temperature threshold for heat wave events. As mean daily temperatures surpass 32.22°C by the late 2050s, the likelihood of any given day surpassing this temperature increases. This might lead to separate events “coalescing” into longer lasting heat waves. It also explains why changes in this metric are much lower in uncorrected data (Figure 5), as temperatures are less likely to reach the heat wave threshold. These results compare favorably with the 35-model ensemble used in the 2015 New York City Panel for Climate Change analysis (Horton et al., 2015), which only corrects for the mean of the temperature distribution (i.e., the *delta method*). However, when correcting for the standard deviation as well, end of century heat waves in RCP8.5 are both longer, and hotter.

The bias correction technique to downscale temperatures from GCM to local scale reduces differences between observation records by reducing biases in both the mean and variance of the model. Applying the technique to each model in the 26-member ensemble results in a reduction, in general, of inter-model spread, as all models are downscaled to the same historical record. This reduction does not hold for event duration, perhaps due to the uncertainty of event timing in addition to daily maximum temperatures involved in this metric. Another limitation of this approach is the assumption that the relationship between observations and GCM output will remain stationary for the entire projection period (Dixon et al., 2016), which might not account for feedback processes such as additional anthropogenic heat and soil desiccation or moistening.

To partially address some of these limitations, we conducted a set of simulations using a state-of-the-art high resolution urbanized regional climate model. This model depends on formulations of physical processes including many of the urban surface-atmosphere feedbacks that may modify heat wave conditions, rather than statistical relationships developed *a priori* or assumptions about the stationarity of bias correction parameters. These assumptions are particularly relevant for projections in NYC, as it has been shown that the stationarity assumption may be violated in coastlines and especially in warm projections (Lanzante et al., 2018), where grid cells may contain water, which in turn modifies near surface temperatures.

### 3.3. High resolution urbanized simulations

High resolution regional climate models have been used to improve representation of precipitation and temperature (Antic et al., 2004; El-Samra et al., 2017; Garuma et al., 2018; Hughes et al., 2017; Miller et al., 2008), especially in locations where complex surface processes are significant (e.g., mountains, coasts, and cities), although some studies have found geographically inconsistent accuracy improvements (Wang and Kotamarthi, 2015). In addition, high resolution dynamical downscaling methods have been used to derive projections of extreme events, such as heat waves (Gao et al., 2012). Here, we employ advances in the representation of urban physics in the WRF model to project heat wave metrics throughout NYC. Our simulation approach focuses on three time periods representing contemporary (2006-2010), mid-century (2045-2049), and end of century (2095-2099) across the RCP4.5 and RCP8.5 scenarios.

Evaluating model output against weather station data (Central Park, LGA, and JFK) for the contemporary period (2006-2010) reveals that WRF simulated daily maximum temperature improves on the input bias corrected Community Earth System Model (BC-CESM1) input

data in both model mean and standard deviation (Figure 6a). Observations reported a mean daily maximum of 28.41°C with a standard deviation of 3.69°C. WRF simulations results, interpolated to weather station locations using nearest neighbor showed a mean daily maximum of 28.66°C (0.25°C error) with a 3.37°C standard deviation (0.32 error), whereas BC-CESM1 showed a 26.54°C mean (1.87°C error) and 2.87°C standard deviation (0.82°C% error). These results are consistent with other studies (Bruyère et al., 2014), which found reduced cold biases in near surface temperature distributions when forcing WRF with bias-corrected climate data.

On the other hand, mean daily minimum temperatures (Figure 6b) are overestimated by both BC-CESM1 and WRF simulations by 1.38 and 2.54°C, respectively. WRF simulations, however, improve on standard deviation, with an error of 0.04°C, while in BC-CESM1 the error reaches 0.31°C. Both WRF and BC-CESM1 reproduce the Weibull distribution of the 10 m winds. However, WRF underestimates calm wind conditions (<5 m/s), while slightly overestimating wind speeds >6 m/s compared to BC-CESM1. WRF does capture extreme wind conditions, with BC-CESM only reaching a maximum of 10 m/s, whereas WRF reaches up to 18 m/s, closer to the observed maximums of 22 m/s.

Limitations in BC-CESM1 are, in part, inherent to its coarse horizontal resolution (0.94 latitude × 1.24 longitude, ~100 km near NYC). Locations near the coast are especially vulnerable to these limitations, as a grid cell's area of influence includes both land and water, impacting its ability to reproduce observed temperature variance (Lanzante et al., 2018).

### [Figs. 6-7]

Mean heat wave intensity (Figure 7, left) projections show, in general, larger increases closer to the coast compared to inland locations. In the RCP4.5, heat wave intensity peaks in the mid-century period, with most of the city experiencing increases between 0-3°C. Increases are largest over the southeast part of the city, suggesting a weakening of the afternoon sea

breeze (Figure 8) that would typically keep this location cooler, as seen from the JFK station records (Figure 3). By end of century, meant event intensity ranges between 0.5 to 2°C, following a similar geographical pattern. In RCP8.5, event intensity increases throughout the century, with the largest anomalies observed in the latter half, similar to results in the statistically downscaled projections. Here, however, intensity anomalies range from 2-5°C. As shown in Figure 8, simulations show an overall reduction in wind speeds. During the 10% coolest days, wind direction distribution is fairly similar, with southeast and southwesterly winds flow being the most common, albeit with an end of century reduction from 2.0-3.2 m/s to 1.2-2.8 m/s. During the 10% warmest days, end-of-century wind directions exhibit a shift closer to southwesterly flows, potentially due, in part, to increased urban-rural temperature gradients. Warm days also show a similar wind speed reduction as in the 10% coolest days, marking an overall weakening of flow over the city, which may lead to increased UHI magnitudes as shown by previous studies (Founda and Santamouris, 2017; Li et al., 2016).

### [Fig. 8]

Mean event duration (Figure 7, right) anomalies display an almost opposite geospatial gradient compared to event intensity, with larger increases over Manhattan (west part of the city). In RCP4.5, events are projected to last 1-3 days longer than the contemporary period across both mid and end of century, albeit with shifts in the location of the maxima. In RCP8.5, the mean event duration follows a similar geospatial pattern between mid-century and end of century as that of RCP4.5, reaching more than 7 additional events. However, as in the single point projections, “coalescing events” are more likely to occur in RCP8.5. Excess heat wave days in densely packed parts of the city suggest that as summers become warmer, heat stored in buildings may play a role in extending event duration. In particular, lack of evapotranspiration due to impervious surfaces as well as heat storage in built structures may extend heat wave conditions heterogeneously throughout the city, coupled with increased

anthropogenic heat from air conditioning. This heterogeneity is particularly important due to geographical differences in socioeconomic status of residents, translating to a difference in risk of heat impacts to health.

Studies have shown that water vapor content of air, in addition to ambient temperature, regulates the ability of humans to cool down via evaporation of sweat (Malchaire et al., 2000). Simulated projections of water vapor mixing ratio changes (Figure 9a) appear to be sensitive to distance to the coast, as sea breeze circulations bring moist ocean air to the city. Moreover, air conditioning systems contribute a portion of anthropogenic heat through evaporative cooling, further increasing atmospheric water vapor. Modeled changes increase with distance to the southern Long Island coastline, since warm air is able to hold more water, and this leads to increases in atmospheric water vapor. In the medium-emissions scenario (RCP4.5), water vapor increases range between 0-14% across simulations 2045-2049, increasing to 6-18% by 2095-2099. In RCP8.5, mid-century changes are less than 4%, but balloon to 24-30% by end of century. The water vapor increases at the end of the century are larger closer to the coast potentially due to increased evaporation over the ocean. Relative humidity, which measures the saturation of the atmosphere to water vapor, is projected to increase in all simulation periods and scenarios, except in end of century RCP8.5 (Figure 9b). This decrease indicates that capacity of air to carry water vapor, a function of temperature, is increasing at a faster pace than vapor is being added.

### [Fig. 9]

#### 4. Conclusions

Use of dynamical downscaling techniques accounts for statistical methods' shortcomings by improving resolution, and thus representation of heterogeneous urban surfaces, as well as inclusion of urban-specific processes. However, these new methods are computationally

intensive, limiting the feasibility of multi-model, full year ensembles, which are useful to better quantify projection uncertainties. Additionally, there are uncertainties in the temporal change of urban parameters such as land cover, building height or building technology (e.g. higher air conditioning efficiency and improved thermal performance), which might modify urban-atmosphere interactions.

Lack of detailed information on parameters such as air conditioning adoption throughout the city and even building occupancy schedules may also impact anthropogenic heat fluxes, necessitating partnerships with stakeholders at the building and city levels. As cities become more aware of upcoming challenges, however, they have started to enact laws to collect this information. One such example in NYC is *Local Law 84 of 2009*, which mandates reporting of energy end use by buildings above certain loads. Research tools have also started to address these issues, as in the work of Xu et al (2018), which introduces a “cooled fraction” parameter to BEM simulations.

Another limitation of this study is the assumption of a static urban canopy; no urban densification or impacts of population shifts are included. These limitations may be addressed with the use of city land cover and building projections, in turn highlighting the need for engagement with policymakers. Krayenhoff et al (2018) offers a recent example of this approach, finding a geographically varying non-linear relationship between urban expansion and global climate change signals throughout the US. Techniques such as cellular automata models of urban land cover sprawl (Clarke et al., 1997; Li and Yeh, 2002; Mitsova et al., 2011) may be incorporated into high resolution simulations, as well as projections of building technology change to account for increases in cooling technology efficiency. Urban expansion and densification has been shown to contribute to local warming, in some instances, as much as warming associated with global climate change, as studies in Paris (Lemonsu et al., 2015), Japan (Adachi et al., 2012), Arizona (Georgescu et al., 2012), and

Sydney (Argüeso et al., 2014) have shown, as does upwind urbanization (Zhang et al., 2009). Atmospheric water vapor projections showed overall increase across all scenarios and RCP's. However, future temperature increases in the dynamically downscaled CESM1 RCP8.5 scenario lead to higher capacity of air to hold water vapor, leading a decrease in relative humidity. This decrease may have considerable health impacts, as skin evaporative cooling via perspiration may not be as inhibited as in RCP4.5 and mid-century RCP8.5. These results do not imply, however, less risk of heat related mortality, as RCP8.5 still has large temperature increases compared to other scenarios.

The approach presented here provides useful insights on the interplay between regional and local climate and the potential for localized intensification of extreme heat. These insights may be useful for city-level stakeholders for planning of adaptation strategies for health and energy and may serve as a template for projections of extreme heat metrics for other cities.

## References

- Adachi, S. A., Kimura, F., Kusaka, H., Inoue, T., Ueda, H. 2012. Comparison of the Impact of Global Climate Changes and Urbanization on Summertime Future Climate in the Tokyo Metropolitan Area. *Journ. of Appl. Met. and Clim.*, **51(8)**: 1441-1454. doi: 10.1175/JAMC-D-11-0137.1
- Anderson, G. B., Bell, M. L. 2010. Heat waves in the United States: Mortality risk during heat waves and effect modification by heat wave characteristics in 43 U.S. Communities. *Env. Health Persp.*, **119(2)**: 210-218. doi: 10.1289/ehp.1002313
- Anderson, G. B., Bell, M. L. 2012. Lights Out: Impact of the August 2003 Power Outage on Mortality in New York, NY. *Epidem.*, **23(2)**: 189-193. doi: 10.1097/EDE.0b013e318245c61c
- Antic, S., Laprise, R., Denis, B., de Elía, R. 2004. Testing the downscaling ability of a one-way nested regional climate model in regions of complex topography. *Clim. Dyn.*, **23(5)**: 473-493. doi: 10.1007/s00382-004-0438-5
- Argüeso, D., Evans, J. P., Fita, L., Bormann, K. J. 2014. Temperature response to future urbanization and climate change. *Clim. Dyn.*, **42(7-8)**: 2183-2199. doi:

10.1007/s00382-013-1789-6

- Bruyère, C. L., Done, J. M., Holland, G. J., Fredrick, S. 2014. Bias corrections of global models for regional climate simulations of high-impact weather. *Clim. Dyn.*, **43(7-8)**: 1847-1856. doi: 10.1007/s00382-013-2011-6
- Clarke, K. C., Hoppen, S., Gaydos, L. 1997. A self-modifying cellular automaton model of historical urbanization in the San Francisco Bay area. *Env. and Plan. B: Plan. and Des.*, **24(2)**: 247-261. doi: 10.1068/b240247
- Dixon, K. W., Lanzante, J. R., Nath, M. J., Hayhoe, K., Stoner, A., Radhakrishnan, A., Balaji, V., Gaitán, C. F. 2016. Evaluating the stationarity assumption in statistically downscaled climate projections: is past performance an indicator of future results? *Clim. Change*, **135(3-4)**: 395-408. doi: 10.1007/s10584-016-1598-0
- El-Samra, R., Bou-Zeid, E., El-Fadel, M. 2017. To what extent does high-resolution dynamical downscaling improve the representation of climatic extremes over an orographically complex terrain? *Theo. and Appl. Clim.*. doi: 10.1007/s00704-017-2273-8
- Founda, D., Santamouris, M. 2017. Synergies between Urban Heat Island and Heat Waves in Athens (Greece), during an extremely hot summer (2012). *Sci. Reports*, **7(1)**. doi: 10.1038/s41598-017-11407-6
- Gaffin, S. R., Rosenzweig, C., Khanbilvardi, R., Parshall, L., Mahani, S., Glickman, H., Goldberg, R., Blake, R., Slosberg, R. B., Hillel, D. 2008. Variations in New York city's urban heat island strength over time and space. *Theo. and Appl. Clim.*, **94(1-2)**: 1-11. doi: 10.1007/s00704-007-0368-3
- Gao, Y., Fu, J. S., Drake, J. B., Liu, Y., Lamarque, J.-F. 2012. Projected changes of extreme weather events in the eastern United States based on a high-resolution climate modeling system. *Env. Res. Letts.*, **7(4)**: 044025. doi: 10.1088/1748-9326/7/4/044025
- Garuma, G. F., Blanchet, J.-P., Girard, É., Leduc, M. 2018. Urban surface effects on current and future climate. *Urb. Clim.*, **24**: 121-138. doi: 10.1016/j.uclim.2018.02.003
- Gedzelman, S. D., Austin, S., Cermak, R., Stefano, N., Partridge, S., Quesenberry, S., Robinson, D. A. 2003. Mesoscale aspects of the urban heat island around New York City. *Theo. and Appl. Clim.*, **75(1-2)**: 29-42. doi: 10.1007/s00704-002-0724-2
- Georgescu, M., Moustaqui, M., Mahalov, A., Dudhia, J. 2012. Summer-time climate impacts of projected megapolitan expansion in Arizona. *Nat. Clim. Change*, **3(1)**: 37-41. doi: 10.1038/nclimate1656
- Gutiérrez, E., González, J. E., Martilli, A., Bornstein, R. 2015a. On the anthropogenic heat

- fluxes using an air conditioning evaporative cooling parameterization for mesoscale urban canopy models. *Journ. of Sol. Energy Eng'g*, **137(5)**: 051005. doi: 10.1115/1.4030854
- Gutierrez, E., Martilli, A., Ramamurthy, P., González, J. 2016. A modeling approach for the estimation of latent heat fluxes in urban environments: Implementation and assessment. *Int'l Journ. of Clim.* [Under Review]
- Gutiérrez, E., Martilli, A., Santiago, J. L., González, J. E. 2015b. A Mechanical Drag Coefficient Formulation and Urban Canopy Parameter Assimilation Technique for Complex Urban Environments. *Bound.-Layer Met.*, **157(2)**: 333-341. doi: 10.1007/s10546-015-0051-7
- Hawkins, E., Osborne, T. M., Ho, C. K., Challinor, A. J. 2013. Calibration and bias correction of climate projections for crop modelling: An idealised case study over Europe. *Agri. and Forest Met.*, **170**: 19-31. doi: 10.1016/j.agrformet.2012.04.007
- Hong, S.-Y., Lim, J.-O. J. 2006. The WRF Single-moment 6-class Microphysics Scheme (WSM6). *A-Pac. Journ. of Atm. Sci.*, **42(2)**: 129-151.
- Horton, R., Bader, D., Kushnir, Y., Little, C., Blake, R., Rosenzweig, C. 2015. New York City Panel on Climate Change 2015 Report Chapter 1: Climate Observations and Projections: NPCC 2015 Report Chapter 1. *Ann's of the NY Acad. of Sci.*, **1336(1)**: 18-35. doi: 10.1111/nyas.12586
- Hughes, M., Lundquist, J. D., Henn, B. 2017. Dynamical downscaling improves upon gridded precipitation products in the Sierra Nevada, California. *Clim. Dyn.* doi: 10.1007/s00382-017-3631-z
- Kain, J. S. 2004. The Kain-Fritsch convective parameterization: an update. *Journ. of Appl. Met.*, **43(1)**: 170-181. doi: 10.1175/1520-0450(2004)043<0170:TKCPAU>2.0.CO;2
- Krayenhoff, E. S., Moustaqui, M., Broadbent, A. M., Gupta, V., Georgescu, M. 2018. Diurnal interaction between urban expansion, climate change and adaptation in US cities. *Nat. Clim. Change*, **8(12)**: 1097. doi: 10.1038/s41558-018-0320-9
- Lanzante, J. R., Dixon, K. W., Nath, M. J., Whitlock, C. E., Adams-Smith, D. 2018. Some Pitfalls in Statistical Downscaling of Future Climate. *Bull. of the Am. Met. Soc.*, **99(4)**: 791-803. doi: 10.1175/BAMS-D-17-0046.1
- le Comte, D. M., Warren, H. E. 1981. Modeling the impact of summer temperatures on national electricity consumption. *Journ. of Appl. Met.*, **20(12)**: 1415-1419. DOI: 10.1175/1520-0450(1981)020<1415:MTIOST>2.0.CO;2
- Lemonsu, A., Viguié, V., Daniel, M., Masson, V. 2015. Vulnerability to heat waves: Impact of

- urban expansion scenarios on urban heat island and heat stress in Paris (France). *Urb. Clim.*, **14**: 586-605. doi: 10.1016/j.uclim.2015.10.007
- Li, D., Bou-Zeid, E. 2013. Synergistic interactions between urban heat islands and heat waves: The impact in cities is larger than the sum of its parts. *Journ. of Appl. Met. and Clim.*, **52(9)**: 2051-2064. doi: 10.1175/JAMC-D-13-02.1
- Li, D., Sun, T., Liu, M., Wang, L., Gao, Z. 2016. Changes in Wind Speed under Heat Waves Enhance Urban Heat Islands in the Beijing Metropolitan Area. *Journ. of Appl. Met. and Clim.*, **55(11)**: 2369-2375. doi: 10.1175/JAMC-D-16-0102.1
- Li, T., Horton, R. M., Kinney, P. L. 2013. Projections of seasonal patterns in temperature-related deaths for Manhattan, New York. *Nat. Clim. Change*, **3(8)**: 717-721. doi: 10.1038/nclimate1902
- Li, X., Yeh, A. G.-O. 2002. Neural-network-based cellular automata for simulating multiple land use changes using GIS. *Int'l Journ. of Geo. Info. Sci.*, **16(4)**: 323-343. DOI: 10.1080/13658810210137004
- Malchaire, J., Kampmann, B., Havenith, G., Mehnert, P., Gebhardt, H. J. 2000. Criteria for estimating acceptable exposure times in hot working environments: a review. *Int'l Archives of Occup'l and Env. Health* **73(4)**: 215-220. doi: 10.1007/s004200050420
- Martilli, A., Clappier, A., Rotach, M. W. 2002. An urban surface exchange parameterisation for mesoscale models. *Bound.-Layer Met.*, **104(2)**: 261-304.
- Meehl, G. A., Tebaldi, C. 2004. More intense, more frequent, and longer lasting heat waves in the 21st century. *Sci.*, **305(5686)**: 994-997. doi: 10.1126/science.1098704
- Menne, M. J., Durre, I., Vose, R. S., Gleason, B. E., Houston, T. G. 2012. An Overview of the Global Historical Climatology Network-Daily Database. *Journ. of Atm. and Ocea. Tech.*, **29(7)**: 897-910. DOI: 10.1175/JTECH-D-11-00103.1.
- Miller, N. L., Hayhoe, K., Jin, J., Auffhammer, M. 2008. Climate, extreme heat, and electricity demand in California. *Journ. of Appl. Met. and Clim.*, **47(6)**: 1834-1844. doi: 10.1175/2007JAMC1480.1
- Mitsova, D., Shuster, W., Wang, X. 2011. A cellular automata model of land cover change to integrate urban growth with open space conservation. *Landsc. and Urb. Plan.*, **99(2)**: 141-153. doi: 10.1016/j.landurbplan.2010.10.001
- Monaghan, A. J., Steinhoff, D. F., Bruyere, C. L., Yates, D. 2014. NCAR CESM Global Bias-Corrected CMIP5 Output to Support WRF/MPAS Research. UCAR/NCAR-Research Data Archive. doi: 10.5065/D6DJ5CN4
- Nakanishi, M., Niino, H. 2006. An Improved Mellor-Yamada Level-3 Model: Its Numerical

- Stability and Application to a Regional Prediction of Advection Fog. *Bound.-Layer Met.*, **119(2)**: 397-407. doi: 10.1007/s10546-005-9030-8.
- National Weather Service. 2015. *NWS Weather Fatality, Injury and Damage Statistics*.
- National Weather Service. 2018. *NWS New York, NY Excessive Heat Page*.
- Oke, T. R. 1988. The urban energy balance. *Prog. in Phys. Geog.*, **12(4)**: 471–508. doi: 10.1177/030913338801200401
- Ortiz, L., González, J. E., Lin, W. 2018a. Climate change impacts on peak building cooling energy demand in a coastal megacity. *Env. Res. Letts.*, **13(9)**: 094008. doi: 10.1088/1748-9326/aad8d0
- Ortiz, L. E., Gonzalez, J. E., Wu, W., Schoonen, M., Tongue, J., Bornstein, R. 2018b. New York City Impacts on a Regional Heat Wave. *Journ. of Appl. Met. and Clim.*, **57(4)**: 837-851. doi: 10.1175/JAMC-D-17-0125.1
- Piani, C., Weedon, G. P., Best, M., Gomes, S. M., Viterbo, P., Hagemann, S., Haerter, J. O. 2010. Statistical bias correction of global simulated daily precipitation and temperature for the application of hydrological models. *Journ. of Hydrol.*, **395(3-4)**: 199-215. doi: 10.1016/j.jhydrol.2010.10.024
- Ramamurthy, P., González, J., Ortiz, L., Arend, M., Moshary, F. 2017. Impact of heatwave on a megacity: an observational analysis of New York City during July 2016. *Env. Res. Letts.*, **12(5)**: 054011. doi: 10.1088/1748-9326/aa6e59
- Riahi, K., Rao, S., Krey, V., Cho, C., Chirkov, V., Fischer, G., Kindermann, G., Nakicenovic, N., Rafaj, P. 2011. RCP 8.5—A scenario of comparatively high greenhouse gas emissions. *Clim. Change*, **109(1-2)**: 33. doi: 10.1007/s10584-011-0149-y
- Rosenthal, D. H., Gruenspecht, H. K., Moran, E. A. 1995. Effects of Global Warming on Energy Use for Space Heating and Cooling in the United States. *The Energy Journ.*, **16(2)**: 77-96.
- Salamanca, F., Krpo, A., Martilli, A., Clappier, A. 2010. A new building energy model coupled with an urban canopy parameterization for urban climate simulations—Part I. Formulation, verification, and sensitivity analysis of the model. *Theo. and Appl. Clim.*, **99(3-4)**: 331-344. DOI: 10.1007/s00704-009-0142-9
- Santamouris, M., Papanikolaou, N., Livada, I., Koronakis, I., Georgakis, C., Argiriou, A., Assimakopoulos, D. 2001. On the impact of urban climate on the energy consumption of buildings. *Sol. Energy*, **70(3)**: 201-216. doi: 10.1016/S0038-092X(00)00095-5
- Santiago, J. L., Coceal, O., Martilli, A., Belcher, S. E. 2008. Variation of the Sectional Drag Coefficient of a Group of Buildings with Packing Density. *Bound.-Layer Met.*, **128(3)**:

- 445-457. doi: 10.1007/s10546-008-9294-x
- Schatz, J., Kucharik, C. J. 2015. Urban climate effects on extreme temperatures in Madison, Wisconsin, USA. *Env. Res. Letts.*, **10(9)**: 094024. doi: 10.1088/1748-9326/10/9/094024.
- Scott, A. A., Waugh, D. W., Zaitchik, B. F. 2018. Reduced Urban Heat Island intensity under warmer conditions. *Env. Res. Letts.*, **13(6)**: 064003. doi: 10.1088/1748-9326/aabd6c
- Skamarock, W., Klemp, J., Dudhia, J., Gill, D., Barker, D., Wang, W., Huang, X., Duda, M. 2008. A description of the Advanced Research WRF version 3. DOI: 10.5065/D68S4MVH
- Smith T. T., Zaitchik, B. F., Gohlke, J. M. 2013. Heat waves in the United States: definitions, patterns and trends. *Clim. Change*, **118(3-4)**: 811-825. doi: 10.1007/s10584-012-0659-2
- Taylor, K. E., Stouffer, R. J., Meehl, G. A. 2012. An Overview of CMIP5 and the Experiment Design. *Bull. of the Am. Met. Soc.*, **93(4)**: 485-498. doi: 10.1175/BAMS-D-11-00094.1
- Tewari, M., Chen, F., Wang, W., Dudhia, J., LeMone, M., Mitchell, K., Ek, M., Gayno, G., Wegiel, J., Cuenca, R. 2004. Implementation and verification of the unified NOAH land surface model in the WRF model. paper presented at the 20th conference on weather analysis and forecasting/16th conference on numerical weather prediction. Seattle, WA. 11-15.
- Thomson, A. M., Calvin, K. V., Smith, S. J., Kyle, G. P., Volke, A., Patel, P., Delgado-Arias, S., Bond-Lamberty, B., Wise, M. A., Clarke, L. E., Edmonds, J. A. 2011. RCP4.5: a pathway for stabilization of radiative forcing by 2100. *Clim. Change*, **109(1-2)**: 77. DOI: 10.1007/s10584-011-0151-4
- van Vuuren, D. P., Edmonds, J., Kainuma, M., Riahi, K., Thomson, A., Hibbard, K., Hurtt, G. C., Kram, T., Krey, V., Lamarque, J.-F., Masui, T., Meinshausen, M., Nakicenovic, N., Smith, S. J., Rose, S. K. 2011. The representative concentration pathways: an overview. *Clim. Change*, **109(1-2)**: 5-31. doi: 10.1007/s10584-011-0148-z
- Wang, J., Kotamarthi, V. R. 2015. High-resolution dynamically downscaled projections of precipitation in the mid and late 21st century over North America. *Earth's Future*, **3(7)**: 268-288. doi: 10.1002/2015EF000304.
- Wichansky, P. S., Steyaert, L. T., Walko, R. L., Weaver, C. P. 2008. Evaluating the effects of historical land cover change on summertime weather and climate in New Jersey: Land cover and surface energy budget changes. *Journ. of Geophys. Res.*, **113(D10)**. doi:

10.1029/2007JD008514

Xu, X., Chen, F., Shen, S., Miao, S., Barlage, M., Guo, W., Mahalov, A. 2018. Using WRF-Urban to Assess Summertime Air Conditioning Electric Loads and Their Impacts on Urban Weather in Beijing. *Journ. of Geophys. Res: Atms.* doi: 10.1002/2017JD028168.

Zhang, D.-L., Shou, Y.-X., Dickerson, R. R. 2009. Upstream urbanization exacerbates urban heat island effects. *Geophys. Res. Letts.*, **36(24)**. doi: 10.1029/2009GL041082

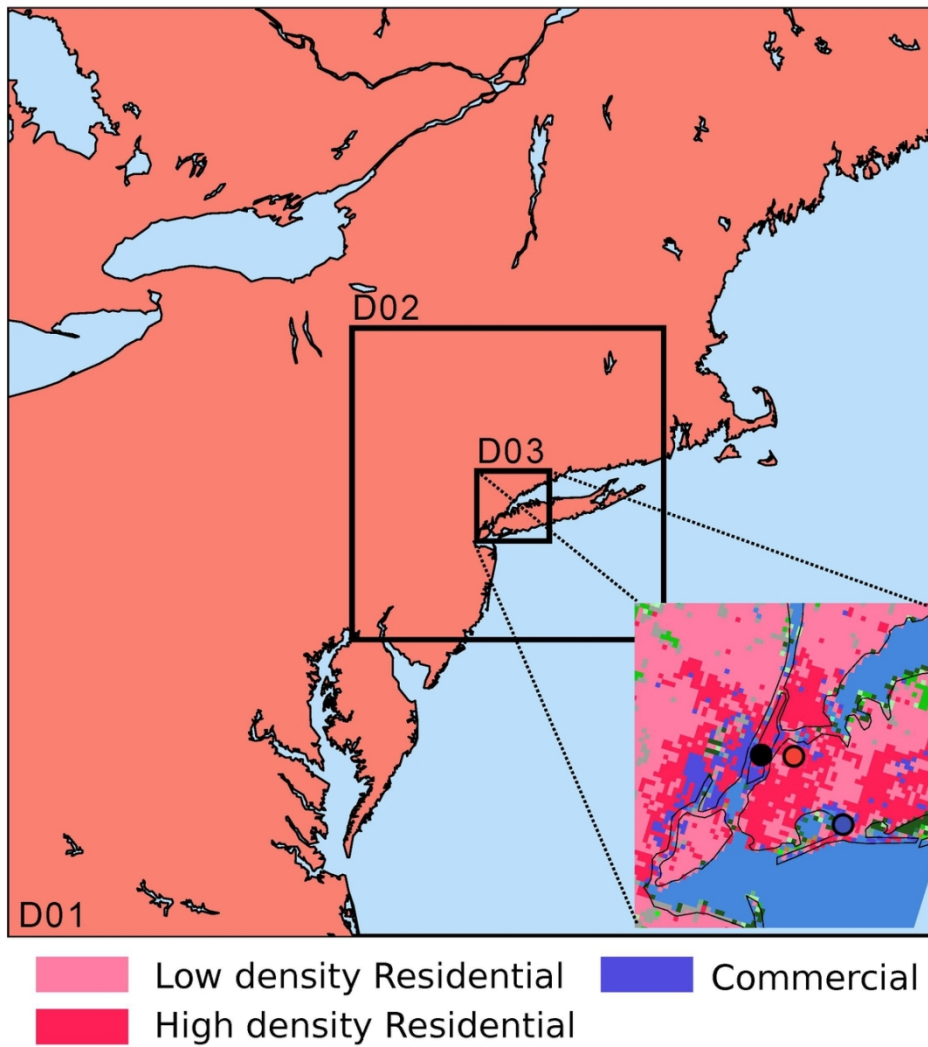


Figure 1. Dynamical downscaling parent (D01) and nested domains (D02, D03) used in all simulations. Insert shows urban PLUTO-derived land use classification for D03. Black, red, and blue circles indicate the location of the Central Park, LGA, and JFK weather stations.

108x116mm (300 x 300 DPI)

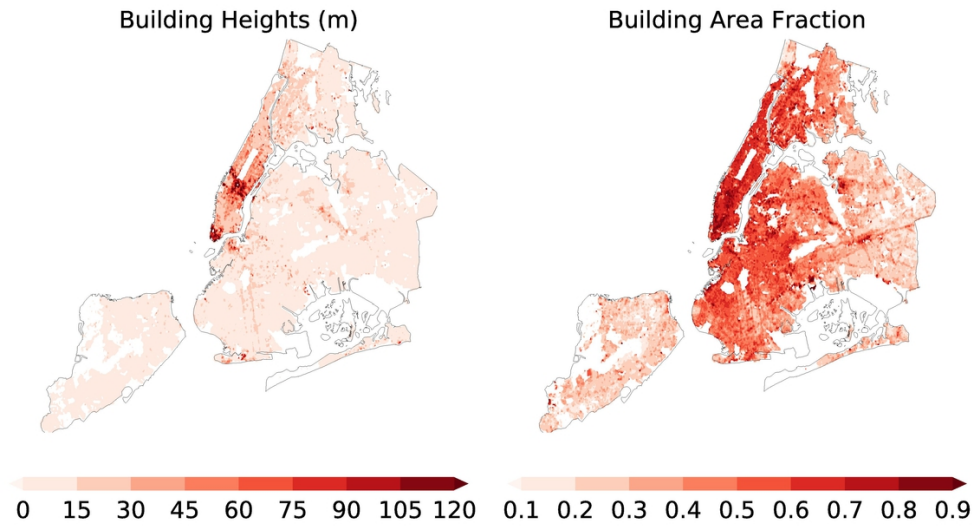


Figure 2. Building plant area fraction (left) and building height (right) parameters used in all simulations. Data is aggregated at 1 km grid spacing before ingesting into the urban WRF model.

97x52mm (300 x 300 DPI)

# ted Article

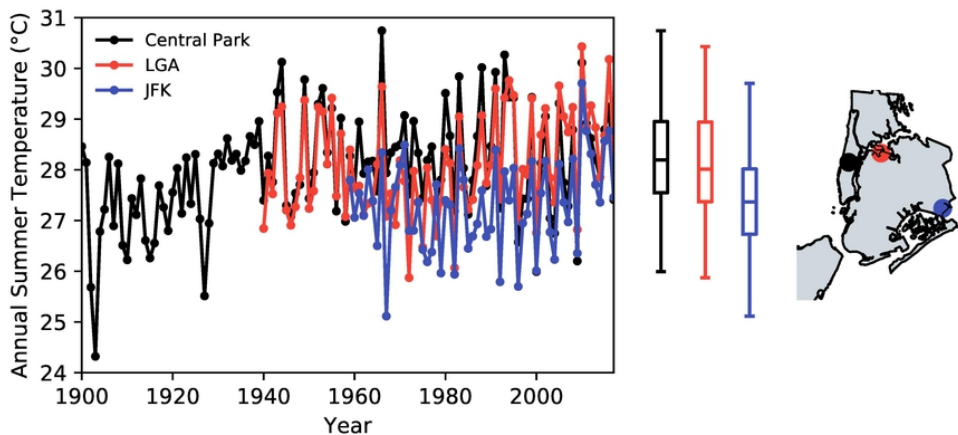


Figure 3. Annual daily maximum temperature trends from the Central Park (40.78N, 73.97W), LaGuardia (40.78N, 73.89W), and John F. Kennedy (40.64N, 73.76W) Airports. Box plots show distribution of annual mean maximum temperatures for the overlapping period recorded by all three stations (1959-2017). Boxes' lower and higher bounds represent each record's 25th and 75th percentiles, with center lines showing its median. Lower and upper whiskers represent data lower and higher than 1.5 times the interquantile range. The map shows each station's geographical location.

75x34mm (300 x 300 DPI)

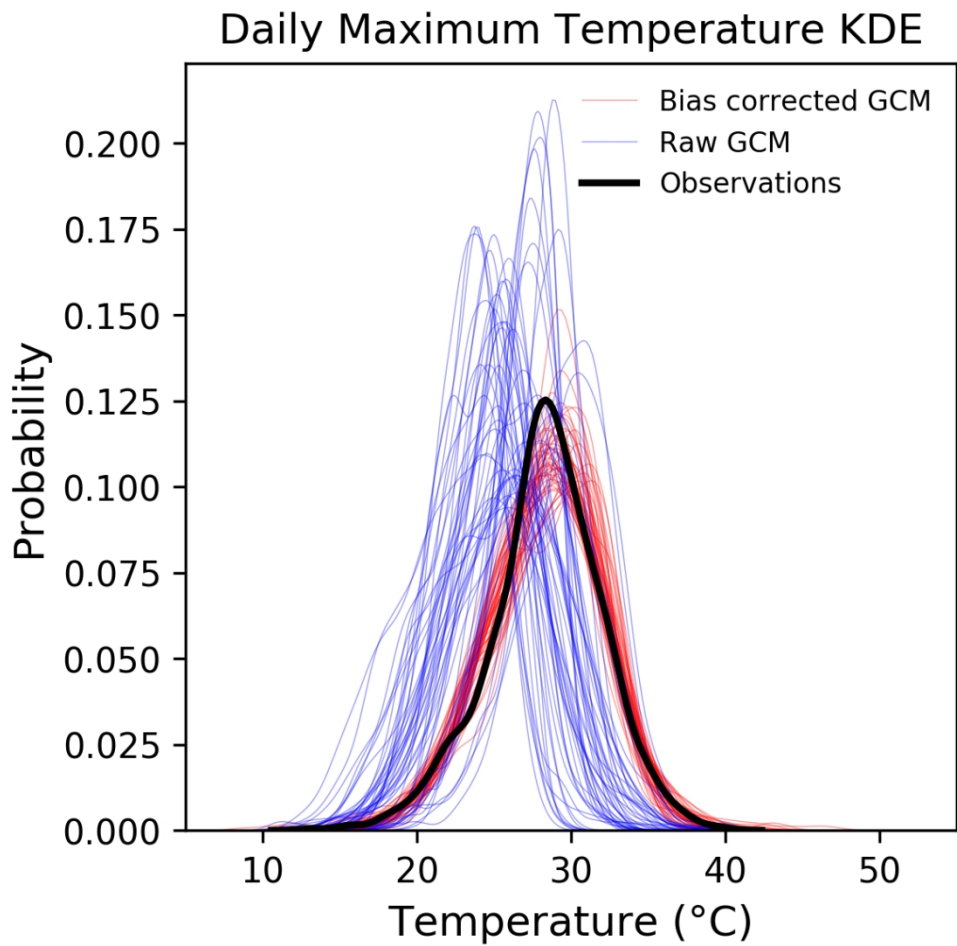


Figure 4. Kernel density estimate (KDE) of 26 model, two- scenario ensemble before (blue) and after (red) histogram matching bias correction. Black curve represents airport observations KDE.

102x100mm (300 x 300 DPI)

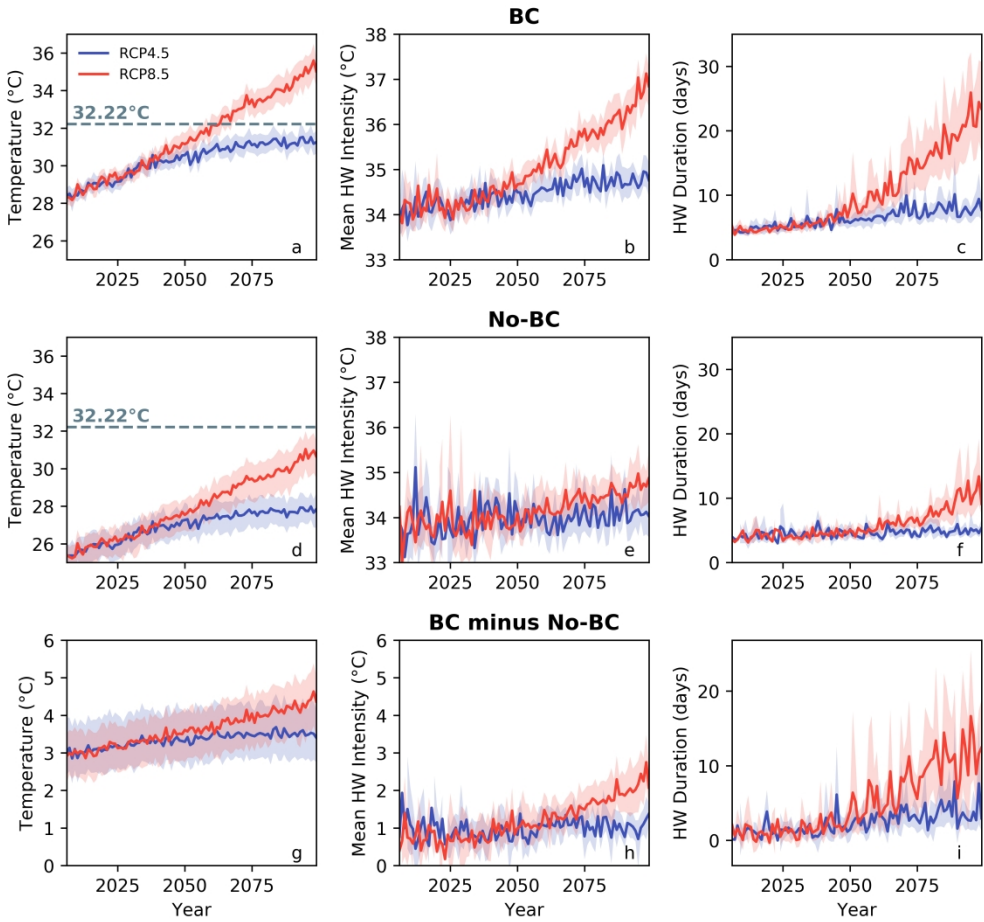


Figure 5. Daily maximum temperature and heat wave metric projections for New York City. Top row show bias-corrected projections of daily maximum temperature (a), mean heat wave intensity (b), and mean heat wave duration (c). Center row (d-f) shows the same metrics from uncorrected data, with the bottom row (g-i) showing the difference the two. Solid blue and red bands indicate the 26 model ensemble mean, with shaded bands representing bootstrapped 95% confidence intervals. Gray dashed lines (a and d) show the temperature threshold for heat waves.

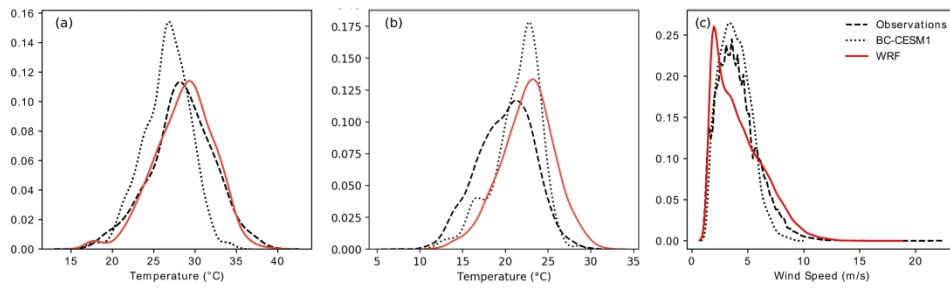


Figure 6. Distribution of modeled and observed (a) daily maximum temperatures, (b) daily minimum temperatures, and (c) daily average wind speed in New York City between 2006 and 2010. Distributions are represented by kernel density estimates of daily maximum temperature. Observations belong to the Central Park, JFK, and LGA Global Historical Climatology Network (GHCN) stations. BC-CESM1 refers to CESM1 bias mean-corrected dataset used as initial and boundary conditions in the high resolution simulations, where the closest land grid point to New York City was used. WRF refers to simulated dynamically downscaled data from grid points closest to the three weather stations.

328x101mm (300 x 300 DPI)

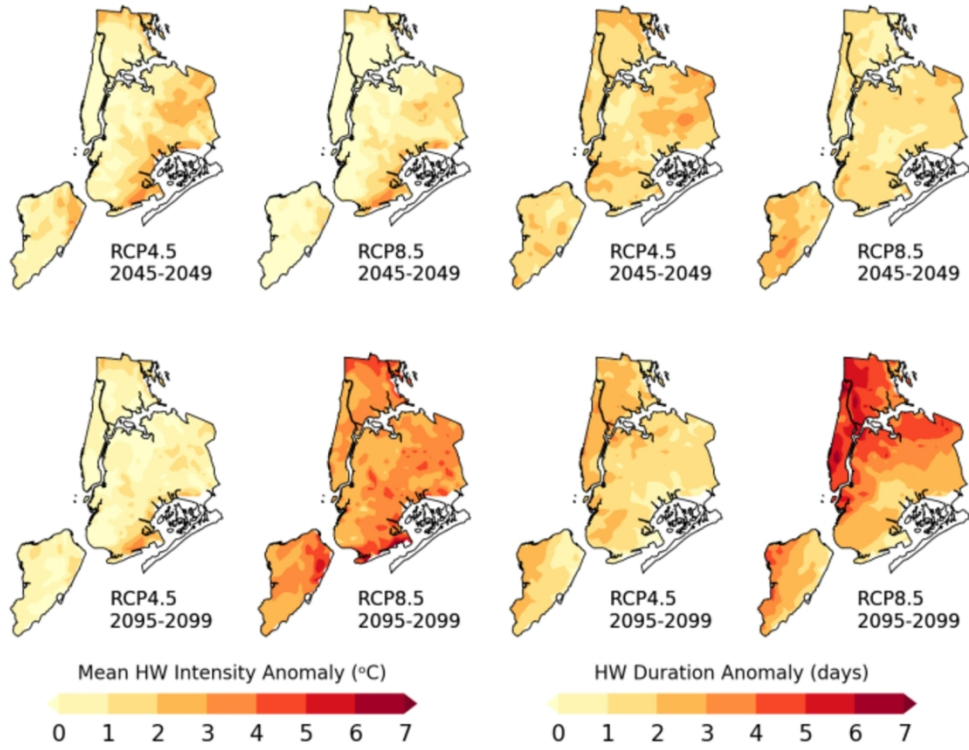


Figure 7. Dynamically downscaled median event intensity (left) and duration (right) for New York City. Anomalies are computed based on simulations of 2006-2010 summers (JJA).

144x111mm (300 x 300 DPI)

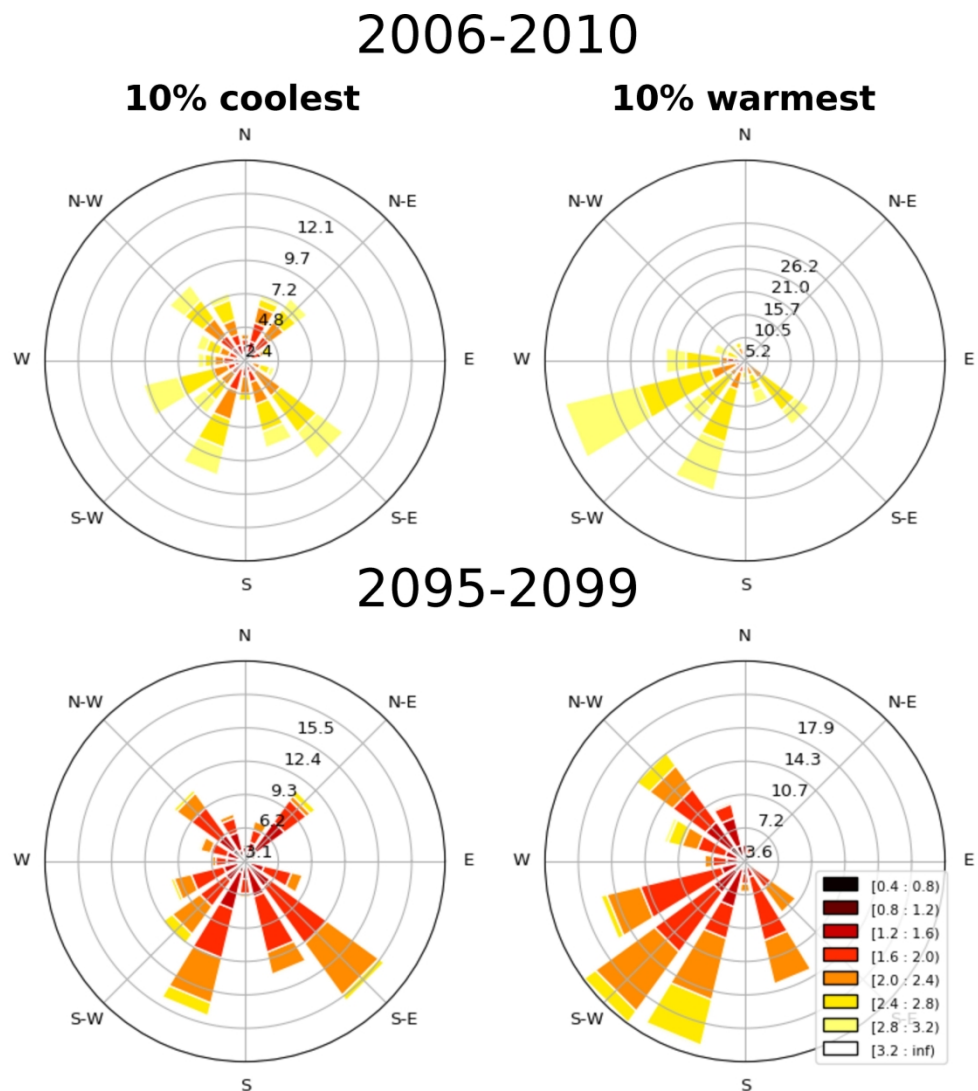


Figure 8. Wind rose plots for selected grid points in Brooklyn, NY. Bar length represents normalized wind direction frequency, while colormap indicates wind speed magnitude.

222x244mm (300 x 300 DPI)

Accepted

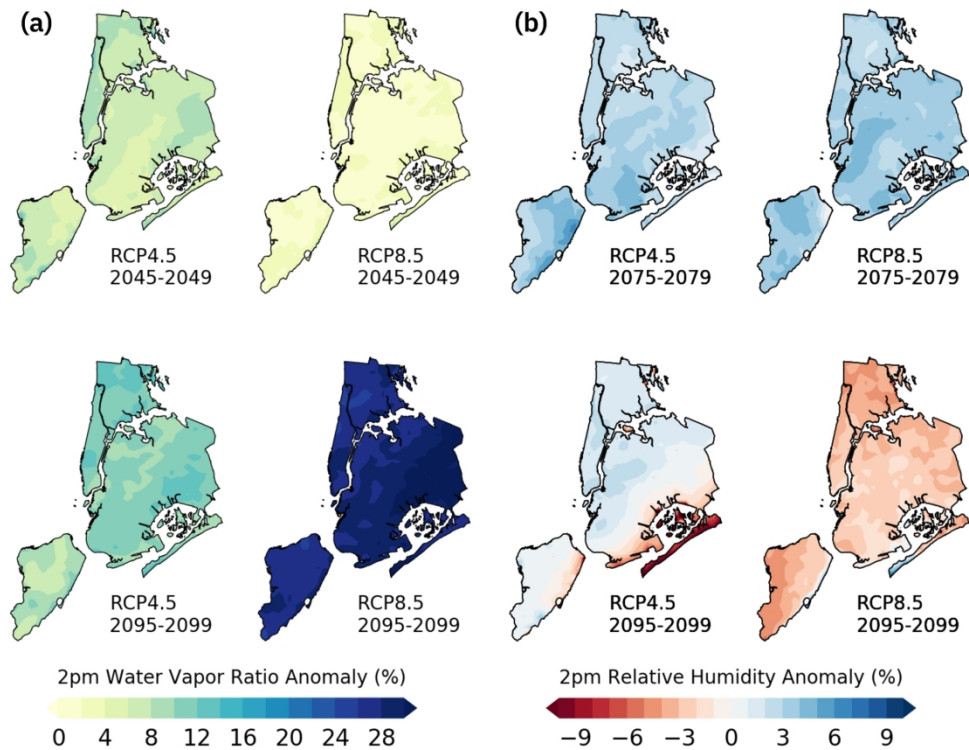


Figure 9. (a) Median 2pm water vapor mixing ratio and (b) relative humidity anomaly over NYC at 2m height.

186x144mm (300 x 300 DPI)

Table 1: 26 model ensemble and center-of-origin used in single point heat wave projections.

<b>Center</b>	<b>Model</b>	<b>Resolution (Lat. x Long.)</b>	<b>Selected coordinate (Lat., Long.)</b>
Commonwealth Scientific and Industrial Research Organization: Bureau of Meteorology (Australia)	ACCESS1.0	1.25° x 1.875°	41.25°, -73.125°
	ACCESS1.3	1.25° x 1.875°	41.25°, -73.125°
Canadian Centre for Climate Modeling and Analysis (Canada)	CanESM2	2.7906° x 2.8125°	40.46°, -73.125°
National Center for Atmospheric Research (USA)	CCSM4	0.9424° x 1.25°	40.99°, -73.75°
Centro Euro-Mediterraneo per i Cambiamenti Climatici (Italy)	CMCC-CM	0.7484° x 0.75°	40.79°, -74.25°
	CMCC-CMS	3.7111° x 3.75°	40.10°, -73.125°
Centre National de Recherches Météorologiques/Centre Européen de Recherche et de Formation Avancée en Calcul Scientifique (France)	CNRM-CM5	1.4008° x 1.40625°	41.32°, -74.53°
Commonwealth Scientific and Industrial Research Organization/Queensland Climate Change Centre of Excellence (Australia)	CSIRO-Mk3.6.0	1.8653° x 1.875°	40.103°, -73.125°
NOAA Geophysical Fluid Dynamics Laboratory (USA)	GFDL-ESM2G	2.0225° x 2	41.46°, -73.75°
	GFDL-ESM2M	2.0225° x 2°	41.46°, -73.75°
NASA Goddard Institute for Space Studies (USA)	GISS-CM3,	2° x 2.5°	41.0°, -73.75°
	GISS-E2-H,	2° x 2.5°	41.0°, -73.75°
	GISS-E2-R	2° x 2.5°	41.0°, -73.75°
Met Office Hadley Centre (UK)	HadGEM2-AO	1.25° x 1.875°	41.25°, -73.125°
	HadGEM2-CC	1.25° x 1.875°	41.25°, -73.125°
	HadGEM2-ES	1.25° x 1.875°	41.25°, -73.125°
Institut Pierre Simon Laplace (France)	IPSL-CM5A-LR	1.8947° x 3.75°	40.74°, -75.0°
	IPSL-CM5A-MR	1.2676° x 2.5°	40.56°, -75.0°
	IPSL-CM5B-LR	1.8946° x 3.75°	40.74°, -75.0°

---

Japan Agency for Marine-Earth Science and Technology, Atmosphere and Ocean Research Institute/National Institute for Environmental Studies/Japan Agency for Marine-Earth Science and Technology (Japan)	MIROC-ESM MIROC- ESM-CHEM MIROC5	2.7906° x 2.8125° 2.7906° x 2.8125° 1.4008° x 1.40625°	40.46°, -73.125° 40.46°, -73.125° 41.32°, -74.53°
Max Planck Institute for Technology (Germany)	MPI-ESM-LR MPI-ESM- MR	1.8653° x 1.875° 1.8653° x 1.875°	40.103°, -73.125° 40.103°, -73.125°
Meteorological Research Institute (Japan)	MRI-CGCM3	1.12148° z 1.125°	40.93°, -74.25°
Institute for Numerical Mathematics (Rusia)	INM-CM4	1.5° x 2°	41.25°, -74.0°

---

Table 2: Model configuration used for all WRF simulations. Values are presented for domain D03, unless otherwise specified.

Parameter	Value
Spinup ( <i>days</i> )	4
Time step ( <i>seconds</i> , D01, D02, D03))	45, 15, 5
Domain size ( <i>grid points</i> )	85 (north-south), 82 (east-west)
SST update	Daily
Simulation period	June 1– August 31 (plus spinup)

Table 3: Model physics parameterizations used throughout all numerical experiments.

Parameterization	Option	Active domain
Cumulus	Kain-Fritsch (Kain, 2004)	D01, D02
Microphysics	WSM6 (Hong and Lim, 2006: 6)	D01, D02, D03
Boundary Layer	Mellow-Yamada-Janjić (Nakanishi and Niino, 2006)	D01, D02, D03
Land Surface	Noah land surface model (Tewari et al., 2004)	D01, D02, D03
Urban Physics	BEP (Martilli et al., 2002)	D03
	BEM (Salamanca et al., 2010)	
	Cooling Tower (Gutiérrez et al., 2015a) Urban Drag Coefficient (Gutiérrez et al., 2015b)	

Table 4: Yearly trends of heat wave metrics in NYC. Trends are based on records from Central Park GHCN daily data from 1900-2017.

	<i>Trend (1900-2017)</i>	<i>p value</i>
<i>Heat wave frequency (events per year)</i>	.0059	0.76
<i>Mean Heat wave duration (days per event)</i>	.0036	.27
<i>Mean heat wave intensity (°C)</i>	-.0017	.56